MODIS SEMI-ANNUAL REPORT: JAN/01/98 - JUN/30/98

Radiative Transfer Based Synergistic MODIS/MISR Algorithm for the Estimation of Global LAI & FPAR

Contract: NAS5-96061

J. Knjazihhin, Y. Zhang, Y. Tian, N. Shabanov, and R. B. Myneni

Geography Department, Boston University, 675 Commonwealth Avenue, Boston, MA 02215

Summary of the algorithm

The objective of the contract is to develop a radiative transfer based synergistic algorithm for estimation of global leaf area index (LAI) and fraction of photosynthetically active radiation absorbed by vegetation (FPAR). The algorithm consists of a main procedure that exploits the spectral information content of MODIS measurements and the angular information content of MISR measurements to derive accurate estimation of LAI and FPAR. Should this main algorithm fail, a back-up algorithm is triggered to estimate LAI and FPAR using vegetation indices. Both algorithms are capable of executing in MODIS-only or MISR-only mode, should cloud contamination, data frequency and spatial or temporal resolution requirements hinder a joint MODIS/MISR mode of operation. The MODIS-only mode of the algorithm requires a land cover classification that is compatible with the radiative transfer model used in their derivation. Such a classification based on vegetation structure was proposed and it is expected to be derived from the MODIS Land Cover Product. Therefore, our algorithm has interfaces with the MODIS/MISR surface reflectance product and the MODIS Land Cover Product.

Summary of work performed during the first half of 1997 (January through June)

1. A new method to describe non-linear spectral variation of ground reflectance was developed. The Look-up-Table was finalized for use with the at launch MODIS LAI/FPAR algorithm.
2. The MODIS Look-up-Table and algorithm code have been finalized and delivered to the University of Montana. Version 2.1 of the production code has been delivered to GSFC.
3. Prototyping of the LAI/FPAR algorithm with atmospherically corrected SeaWiFS (Sea-viewing Wide Field-of-view Sensor) and LASUR-AVHRR (LAnd SUrface Reflectances derived from the Advanced Very High Resolution Radiometer) data is currently being performed.
4. The functionality of the algorithm and results on global LAI and FPAR fields estimated with the algorithm from the SeaWiFS and LASUR-AVHRR data were presented at the MODIS Science Team Meeting (June 24-26, 1998).
5. Myneni made a presentation on the results of analysis of 14 years of AVHRR NDVI data at the GCTR/LUCC International conference in Barcelona, Spain, in March 1998.
6. Collaborative work with co-MODIS PI E. Vermote on the surface BRDF coupling in the atmospheric correction algorithm is being performed.
7. A comparison of synthetic MODIS canopy reflectance data with SeaWiFS and LASUR data was carried out.
8. A regression analysis of global LAI and FPAR fields estimated with the algorithm from the SeaWiFS and LASUR-AVHRR data was performed.
9. A data bank of leaf optical spectra was assembled from various sources, and was analyzed to obtain the mean and variance spectra for the six biomes used in our algorithms. At launch version of the Look-up-Table are presently being built.

10. The MISR-only version of the algorithm is currently being prototyped with POLDER (Polarization and Directionality of the Earth's Reflectance) data.
11. A new method to avoid numerical instabilities in the MISR FPAR retrieval technique caused by retrieval uncertainties in canopy reflectances was developed. A new version of the MISR LAI/FPAR algorithm, which realizes this method, was delivered to JPL.
12. A section in the MISR Surface Retrieval ATBD, which describes the FPAR retrieval technique, was revised and sent to JPL.

A detailed description of the activities 1 through 3 is presented in the MODIS Quarterly Report, # 6 (JAN/01/98 – MAR/31/98). An electronic version of the presentation at the June 24-26 MODIS Science Team Meeting is available at

http://modarch.gsfc.nasa.gov/MODIS/SCITEAM/199806/agenda.html.

Comparison of the MODIS synthetic canopy reflectances with the LASUR and SeaWiFS data

Figure 1 displays the MODIS synthetic, SeaWiFS and LASUR data in the RED-NIR plane. The shape of the set generated by the synthetic data differs from those generated by the SeaWiFS and LASUR data. Table 1 summarizes variation ranges of some characteristics of canopy reflectances derived from these data sets. One can see that synthetic canopy reflectances at the red spectral band are essentially underestimated.

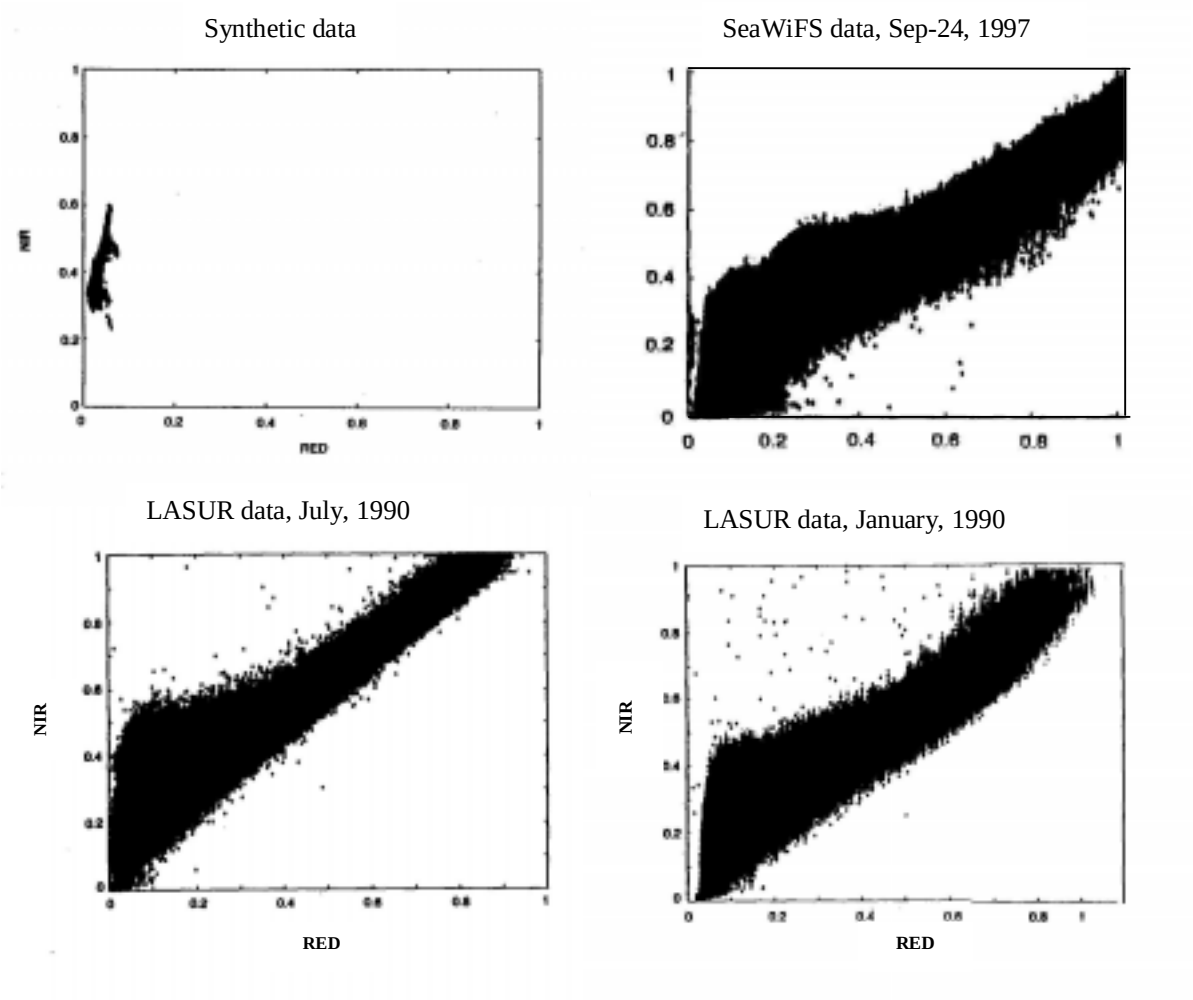

Figure 1. Distribution of pixels with respect to their reflectances at near-infrared and red wavelengths derived from the MODIS synthetic, LASUR and SeaWIFS data sets.

Table 1. Intervals which include 90% of all values of NDVI, Simple Ratio (SM), canopy reflectances at red (RED) and near-infrared (NIR) wavelengths obtained from the MODIS synthetic, LASUR and SeaWiFS data sets.

	Synthetic data	*SeaWiFS (Sep-24)*	*LASUR (July)*	*LASUR (January)*
NDVI	[0.68, 0.92]	[-0.2; 0.6]	[-0.04, 0.8]	[-0.04, 0.8]
SM	[10.0, 26.4]	[0.2, 4.0]	[0.0, 11.6]	[0.0, 11.6]
RED	[0.03, 0.046]	[0.04, 0.89]	[0.03, 0.5]	[0.03, 0.43]
NIR	[0.28, 0.58]	[0.1, 0.9]	[0.1, 0.9]	[0.1, 1.0]

Regression curves

The MODIS LAI/FPAR algorithm is based on the estimation of the LAI distribution function under the condition that the canopy reflectances at the MODIS spectral bands have taken given values. This allows us to treat values of spectral canopy reflectances, their uncertainties, LAI and FPAR as random variables. Statistical techniques, therefore, can be utilized to analyze relationships between measured spectral canopy reflectances and LAI/FPAR retrievals.

Definition. Two curves $x(y)=E(X \mid Y=y)$ and $y(x)=E(Y \mid X=y)$ defined in the (x,y)-*plane* are called the regression curves of X with respect to Y and of Y with respect to X, respectively. Here, X and Y are random variables; $E(X \mid Y=y)$ is expectation of X under the condition that Y has taken the value y. The regression curve has the following interpretation: the best possible prediction of X given a realized value y of Y is $x(y)$. The regression curve $x(y)$ minimizes the expected squared error of the prediction of X on the basis of value of y, and $y(x)$ can be interpreted similarly.

Regression curves were used to analyze the LAI-NDVI and NDVI-FPAR relationships estimated with the MODIS LAI/FPAR algorithm applied to the SeaWiFS and LASUR data as follows. The surface reflectance was treated as a biome dependent random variable. The LASUR and SeaFiFS data were taken as the sets of realizations of this random variable. The LAI/FPAR algorithm was applied to these data in order to evaluate sets of realizations of LAI and FPAR random values. The sets of NDVI realizations were obtained from the LASUR and SeaWiFS data directly. Various regression curves were then derived using these sets.

Let X, Y, and Z be random variables of LAI, NDVI and FPAR values. Figure 2 demonstrates realizations of these random variables in the (LAI, NDVI) [left panel] and (NDVI, FPAR) [right panel] planes. We denote the regression curves of LAI with respect to NDVI and of NDVI with respect to LAI by $x(y)$ and $y(x)$, respectively. Similarly, $z(y)$ and $y(z)$ denote the best possible prediction of FPAR given a realized value y of NDVI and the best possible prediction of NDVI given a realized value z of FPAR. The regressions curves $x(y)$, $y(x)$, $z(y)$ and $y(z)$ for 6 biomes (Grasses and Cereal Crops; Shrubs, Broadleaf Crops; Savannas; Broadleaf Forests; Needle Forests) are shown in Figure 3. The regression curves $x(y)$, $y(x)$ and $z(y)$, $y(z)$ for biome 5 (Broadleaf Crops) are presented in Figure 4. One can see that the curves $y(x)$ and $z(y)$ are close to the inverse function of $x(y)$ and $y(z)$, respectively. This may be taken as evidence of the existence of LAI-NDVI and NDVI-FPAR relationships that have previously been reported in the literature.

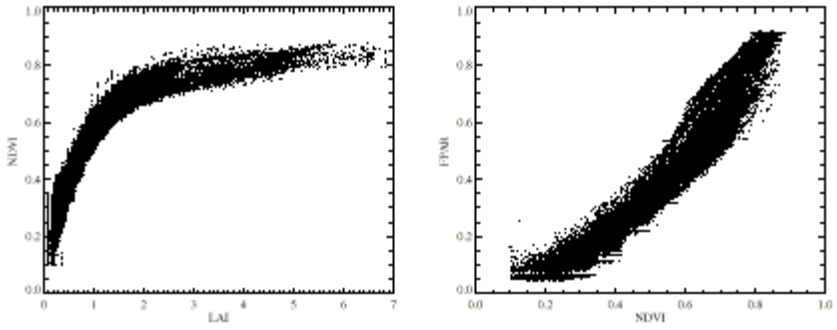

Figure 2. Realizations of LAI (random variable *X*), NDVI (random variable *Y*), and FPAR (random variable *Z*) in the LAI–NDVI [left panel] and NDVI–LAI [right panel] planes generated from the LASUR data.

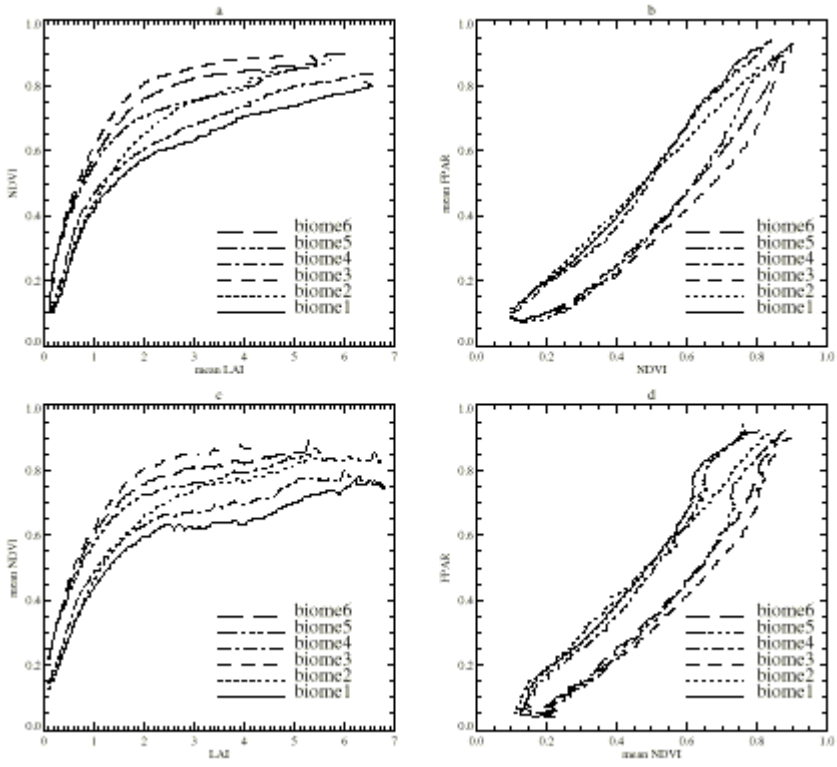

Figure 3. Regression curves for 6 biomes (Grasses and Cereal Crops; Shrubs; Broadleaf Crops; Savannas; Broadleaf Forests; Needle Forests) estimated with the MODIS LAI/FPAR algorithm applied to the LASUR data. Panels (a) and (b): the best possible prediction of LAI and FPAR given a realized value of NDVI. Panels (c) and (d): the best possible prediction of NDVI given realized values of LAI and FPAR.

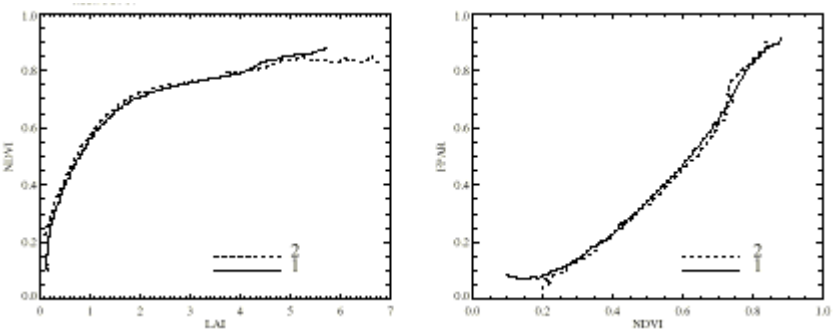

Figure 4. Regression curves for biome 5 (Broadleaf Forests). Left panel: the best possible prediction of LAI, $x(y)$ [curve 1], given a realized value y of NDVI, and the best possible prediction of NDVI, $y(x)$ [curve 2], given a realized value x of LAI. The regression curves $z(y)$ [curve 1] and $y(z)$ [curve 2] are shown in the right panel.

Leaf optical spectra

A key idea of the LAI/FPAR algorithm is the use of the critical eigenvalue to relate canopy structure and spectral leaf albedo. It allows us to compare spectral canopy reflectances with spectral properties of individual leaves, which is a rather stable characteristic of green leaves. Therefore, the leaf optical spectra are a very important element of the Look-up-Table. A data bank of leaf optical spectra was assembled from various sources, and was analyzed to obtained the mean and variance spectra for all biomes used in our algorithm. Figure 5 demonstrates the leaf spectral transmittances (left panels) and reflectances (right panels) for biome 1 (Grasses and Cereal Crops), 5 (Broadleaf Forests) and 6 (Needle Forests). The leaf spectral albedo (reflectance + transmittance) for biome 2 (Shrubs), 3 (Broadleaf Crops) are shown in Figure 6.

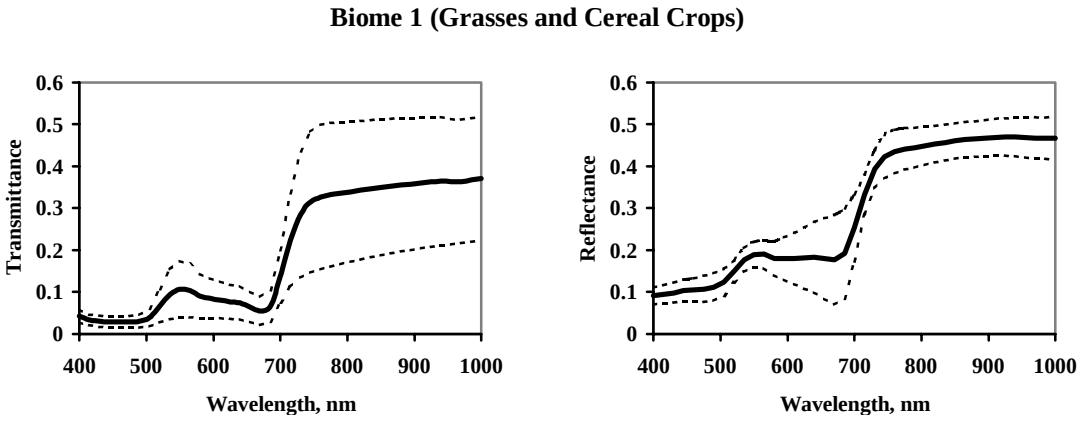

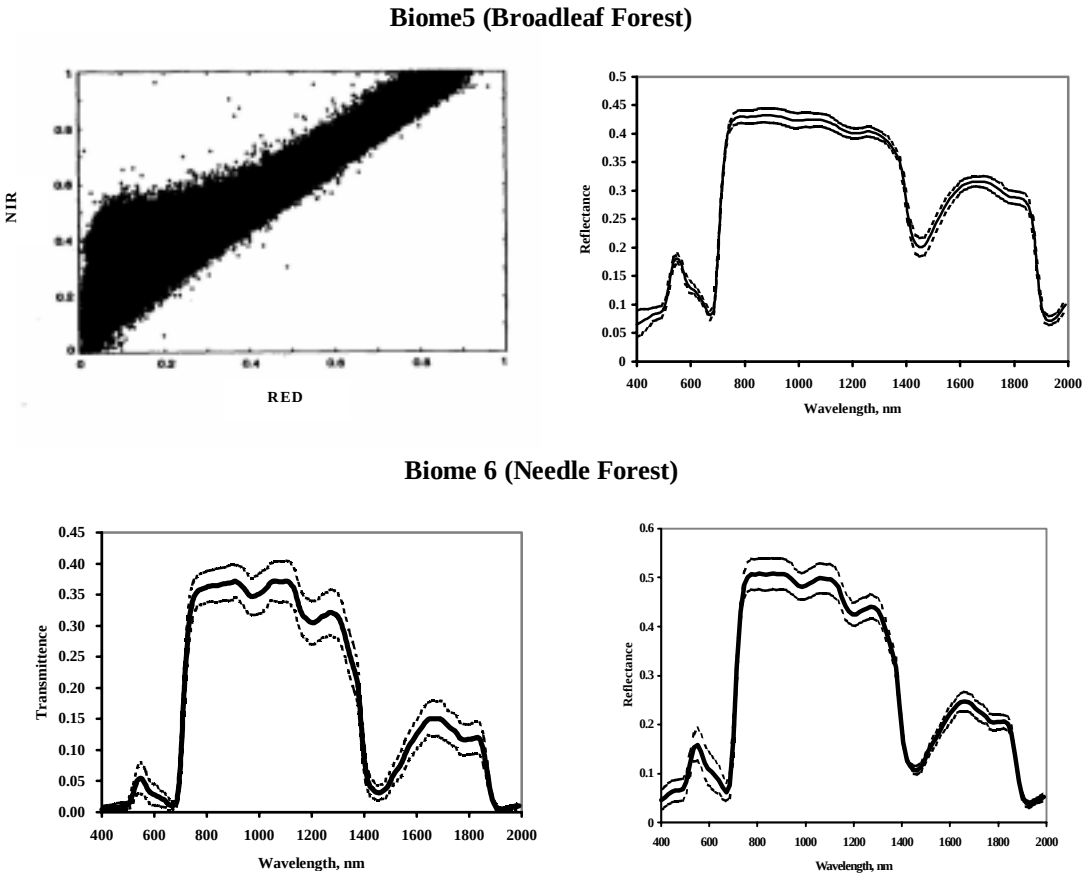

Figure 5. Optical range leaf hemispherical transmittance (left pannels) and reflectance (right pannels) spectra for Grasses and Cereal Crops (biome 1), Broadleaf Forest (Biome 5) and Needle Forest (Biome 6). Means are showhn as solid lines; dotted lines depict ± standart deviation.

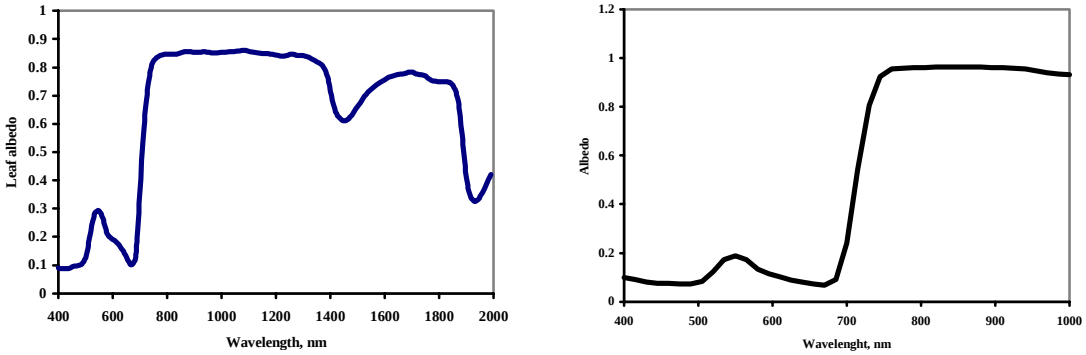

Figure 6. Mean leaf hemispherical albedo for Shrubs (Biome 2) and Broadleaf Crops (biome 3).

Prototyping of the MISR LAI/FPAR algorithm with POLDER data

For each pixel, the POLDER (Polarization and Directionality of the Earth's Reflectance) instrument was designed to provide the atmospherically corrected surface bi-directional reflectance factor (BRF) in up to 14 view directions and at 4 spectral bands (443 nm, 670 nm, 765 nm and 865 nm). We ran both the MISR-only and MODIS-only versions of the LAI/FPAR algorithm using surface reflectances at red and near-infrared wavelengths at about 6 km resolution for the period 1 Nov – 16 Nov 1996.

The MISR-only mode of the algorithm is designed to utilize all the information provided by this instrument, using a two-step process. The first step involves a comparison of the spectral hemispherically integrated reflectances with those determined from the model which depend on biome type, canopy structure and soil/understory reflectances. The biome/canopy/soil/understory models that pass this comparison test are subject to the second step, which is a comparison of their directional reflectances at the MISR angles to the retrieved spectral directional reflectances. Results presented here are obtained by executing the first comparison test. Spatial distribution of spectral hemispherically integrated reflectances was obtained by integrating the BRF values over all view directions available for a given pixel from 1 Nov to 16 Nov, 1996. For each pixel, the MODIS-only mode of the algorithm was executed as many times as number of view angles were available. Results presented here are referred to a site in Central Africa (about 4^{o}N, 22.8^{o}E) covering an area of 600 by 600 km. Figure 7 demonstrates the land cover distribution over this area. Distributions of LAI values estimated with the MODIS-only and MISR-only versions of the algorithm are shown in Figs. 8-10. An analysis of these results will be performed during the next reporting period.

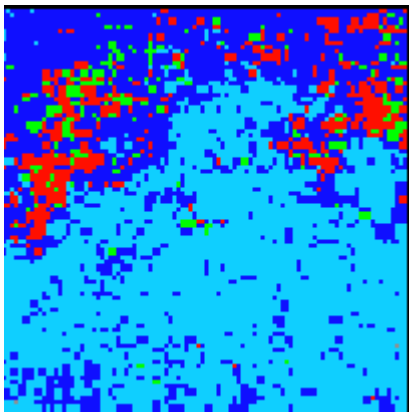

Figure 7. The land cover distribution in a site covering an area of 600x600km located in Central Africa (about 4^{o}N, 22.8^{o}E). The color code is as follows: red is grasses and cereal crops (biome 1), green is broadleaf crops (biome 3), dark blue is savanna, and blue is broadleaf forest (biome 5). This distribution is generated by the Biome Classification MAP and is independent on the POLDER data.

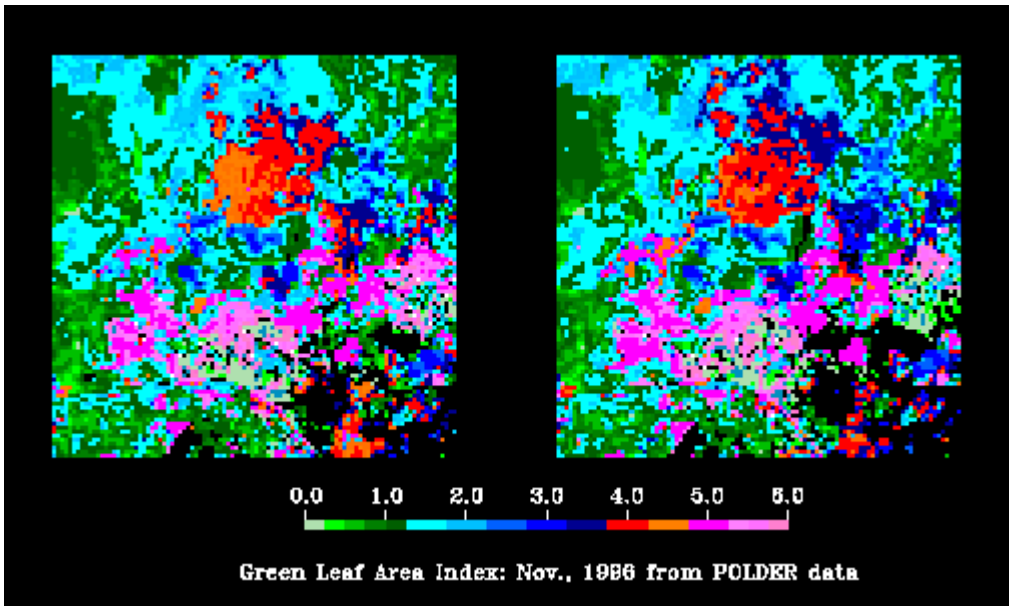

Figure 8. The distribution of LAI on 1 Nov 1996 estimated with the MODIS-only version of the LAI/FPAR algorithm applied to the POLDER data. Two view directions closed to nadir were used to produce this image.

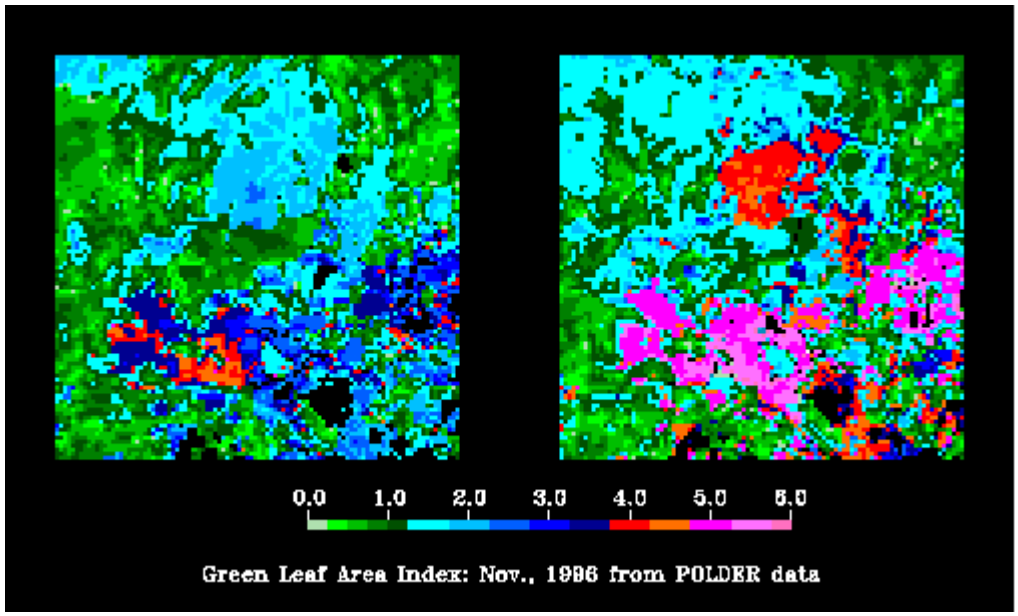

Figure 9. The distribution of LAI on 1 Nov 1996 estimated with the MODIS-only version of the LAI/FPAR algorithm applied to the POLDER data. Two extreme off-nadir view directions were used to to produce this image.

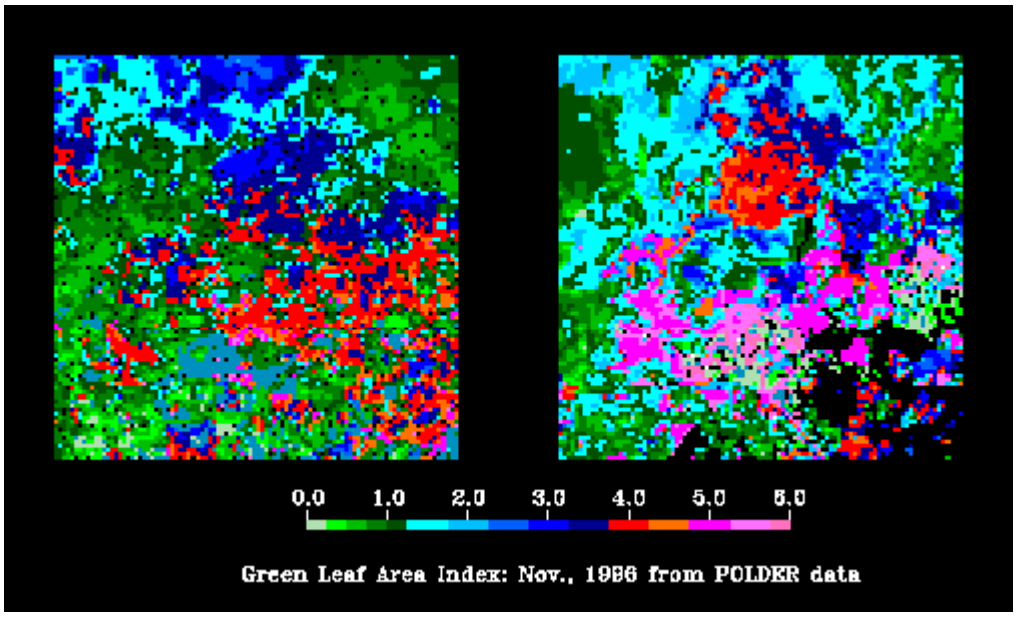

Figure 10. Distribution of LAI values estimated with the MISR-only (left panel) and MODIS-only (right panel) modes of the LAI/FPAR algorithm applied to the POLDER data.

Update to the MISR Surface Retrieval ATBD

When prototyping the MISR-only mode of the LAI/FPAR algorithm it was found that the FPAR retrieval technique is very sensitive to uncertainties in retrieved BHR's (Bi-Hemispherical Reflectance), leading to numerical instabilities in FPAR retrieval. A new method allowing to avoid this problem was proposed. NDVI-FPAR relationship estimated with new MISR FPAR retrieval technique is shown in Figure 11. An update to the MISR Surface Retrieval ATBD, which describes this method, is included as an Appendix to this report.

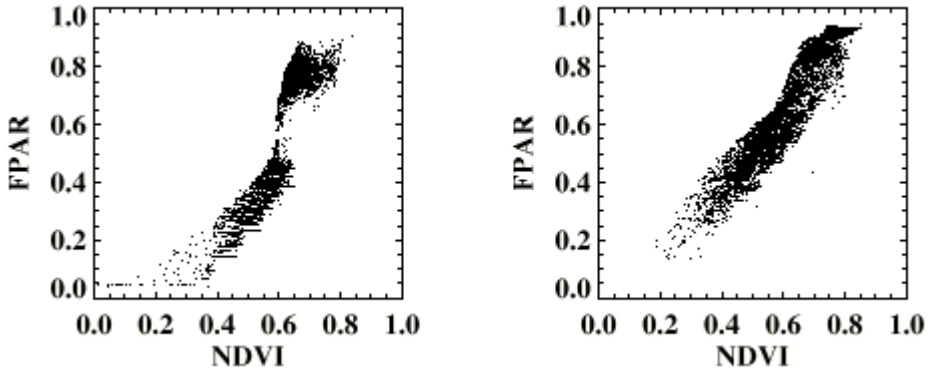

Figure 11. FPAR-NDVI relationships estimated with the MISR-only (left panel) and MODIS-only (right panel) modes of the LAI/FPAR algorithm applied to the POLDER data. The theorem proved in Appendix explains the "break" in the MISR LAI-FPAR relationship which can be removed by decreasing uncertainties both in retrieved BHR's and in canopy radiation models. A view direction closed to nadir was used to derive the MODIS NDVI-FPAR relationship (right panel). The break is not very pronounced in this case. However, the MODIS FPAR retrieval technique, unlike the MISR one, requires the use of a model for the non-linear spectral variation of ground reflectance which makes the retrieved FPAR model dependent. Therefore, the uncertainty in the FPAR retrievals is higher because they result from uncertainties in retrieved surface reflectances, models for canopy radiation regime with ideally black ground and spectral ground reflectance.

Publications

1. Diner, D. J., J.C. Beckert, T.H. Reilly, C.J. Bruegge, J.E. Conel, R. Kahn, R., J.V. Martonchik, T.P. Ackerman, R. Davies, S.A.W. Gerstl, H.R. Gordon, I. P. Muller, R.B. Myneni, P.J. Sellers, B. Pinty, and M.M. Verstraete, Multiangle Imaging SprectroRadiometer (MISR) description and experiment overview, *IEEE Trans. Geosci. Remote Sens.*, 36:1072-1087, 1998.
2. Justice, O., E. Vermote, J.R.G. Townshed, R. Defries, D. P. Roy, D.K. Hall., V.V. Salomonson, J. L. Privette, G. Riggs, A. Strahler, W. Lucht, R.B. Myneni**,** Y. Knyazikhin, S. W. Running, R. R. Nemani, Z. Wan., A. R. Heute, W. van Leeuwen, R. E. Wolfe, L. Giglio, J.-P. Muller, P. Lewis, and M. J. Barnsley, The moderate resolution imaging spectroradiometer (MODIS): Land remote sensing for global research, *IEEE Trans. Geosci. Remote Sens.*, vol. 36, Nr. 4, 1998.
3. Knyazikhin, Y., G. Miessen, O. Panfyorov, R.B. Myneni, and G. Gravenhorst, Influence of vegetation canopy heterogeneity on the interpretation of remotely sensed reflectance measurements, *IEEE Trans. Geosci. Remote Sens*, 1998 (submitted for publication).
4. Knyazikhin, Yu., J. Kranigk, R.B. Myneni, O.Panfyorov, and G.Gravenhorst, 1998. Influence of small-scale structure on radiative transfer and photosynthesis in vegetation cover, *J. Geophys. Res.*, 103(D6), 6133-6144, 1998.
5. Knyazikhin, Yu., J.V. Martonchik, D.J.Diner, R.B. Myneni, M.M. Verstraete, B.Pinty, and N. Gobron, Estimation of vegetation canopy leaf area index and fraction of absorbed photosynthetically active radiation from atmosphere corrected MISR data, *J. Geophys. Res.* 1998 (submitted for publication).
6. Knyazikhin, Yu., J.V., Martonchik, R.B. Myneni, D.J. Diner, and S. Running, Synergistic algorithm for estimating vegetation canopy leaf area index and fraction of absorbed photosynthetically active radiation from MODIS and MISR data. *J. Geophys. Res*, 1998 (submitted for publication).
7. Martonchik, J.V., D.J.Diner, B.Pinty, M.M.Verstraete, R.B.Myneni, Yu.Knyazikhin, and H.R.Gordon, Determination of land and ocean reflective, radiative and biophysical properties using multi-angle imaging, *IEEE Trans. Geosci. Remote Sens.*, 1997 (accepted for publication).
8. Myneni, R. B., C.J. Tucker, G. Asrar, and C.D. Keeling, Interannual variations in satellite-sensed vegetation index data from 1981 to 1991. *J. Geophys. Res.*, 103 (D6): 6145-6160, 1998.

Appendix

3.3.7.2 Mathematical description of the algorithm

FPAR is defined as the fraction of photosynthetically active radiation absorbed by green elements of the vegetation canopy. Therefore,

$$FPAR(bio, lai, \mu_0) = \frac{Q_1(bio, lai, \mu_0) + Q_2(bio, lai, \mu_0)}{E_\lambda(\mu_0)} \quad , \tag{F1}$$

where

$$Q_1(bio, lai, \mu_0) = \int_{400\,\mathrm{nm}}^{700\mathrm{nm}} \mathbf{a}_{bs}^{\mathrm{hem}}(\lambda, bio, lai, \mu_0) e_\lambda^{hem}(\mu_0) E_{0,\lambda}\, d\lambda \quad , \tag{F2}$$

$$Q_2(bio, lai, \mu_0) = \int_{400}^{700} \frac{\mathbf{a}^q(\lambda, bio, lai)}{\mathbf{t}^q(\lambda, bio, lai)} \left[A^{hem}(\lambda, \mu_0) - \mathbf{r}_{bs}^{hem}(\lambda, bio, lai, \mu_0)\right] e_\lambda^{hem}(\mu_0) E_{0,\lambda}\, d\lambda \,, \tag{F3}$$

$$E_\lambda(\mu_0) = \int_{400}^{700} E_{0,\lambda} e_\lambda^{hem}(\mu_0)\, d\lambda \quad . \tag{F4}$$

A derivation of these equations is presented in [MISR Level 2 Ancillary Products and Datasets ATB, Eqs. (95)-(97), (102)]. Here the Q_1 term describes the absorption within the canopy for the case of a black ground and Q_2 describes additional absorption within the canopy due to the interaction between the ground (soil or/and understory) and canopy; $E_{0,\lambda}$ is the TOA solar irradiance spectrum, and e_λ^{hem} is the normalized incident irradiance, defined as the ratio of the radiant energy incident on the surface to $E_{0,\lambda}$ [See Eq. (92)]. These equations underlie the FPAR retrieval technique.

3.3.7.2.1 Influence of uncertainties in BHR retrieval on the evaluation of FPAR

The aim of this subsection is to investigate the sensitivity of canopy absorbtance defined as

$$\mathbf{a}_{\mathrm{model}}^{hem}(\lambda) = \mathbf{a}_{bs}^{hem}(\lambda) + \frac{\mathbf{a}^q(\lambda)}{\mathbf{t}^q(\lambda)} \left[A_{\mathrm{model}}^{hem}(\lambda) - \mathbf{r}_{bs}^{hem}(\lambda)\right] \tag{F5}$$

to the retrieved uncertainties ΔA^{hem} in A^{hem}. In this subsection the angular and *lai* dependencies have been temporarily suppressed in the notations. We use A_{model}^{hem} and $\mathbf{a}_{\mathrm{model}}^{hem}$ to denote the modelled BHR and canopy absorptance; A^{hem} denotes the retrieved value of BHR and $\mathbf{a}^{hem}$ is the estimate of the canopy absorptance using A^{hem}. If we replace the modeled BHR A_{model}^{hem} by its retrieved value A^{hem}, equation (F5) can be violated due to the uncertainty in A^{hem}. We start our analysis with examining the situation when $A^{hem} - \mathbf{r}_{bs}^{hem}$ takes on negative values.

It follows from (101a) and (101d) that if the candidate biome/canopy/soil model passed the first comparison test then

$$\left|A^{hem}(\lambda)-A^{hem}_{\mathrm{mod}el}(\lambda)\right|\le\delta(\lambda) \tag{F6}$$

where $\delta=\Delta A^{hem}\cdot\Delta_{1,\mathrm{thresh}}$. Taking into account (101f), this inequality can be rewritten as

$$\begin{aligned}\mathbf{t}^q(\lambda)\frac{\rho_{q,eff}(\lambda)}{1-\rho_{q,eff}(\lambda)\mathbf{r}^q(\lambda)}\mathbf{t}^{hem,q}_{bs}(\lambda)-\delta(\lambda)\le A^{hem}(\lambda)-\mathbf{r}^{hem}_{bs}(\lambda)\\ \le\mathbf{t}^q(\lambda)\frac{\rho_{q,eff}(\lambda)}{1-\rho_{q,eff}(\lambda)\mathbf{r}^q(\lambda)}\mathbf{t}^{hem,q}_{bs}(\lambda)+\delta(\lambda)\end{aligned}\quad . \tag{F7}$$

It follows from (F7) that the difference $A^{hem}-\mathbf{r}^{hem}_{bs}$ may take on a negative value only if the left side of inequality (F7) is negative, i.e.,

$$\mathbf{t}^q(\lambda)\frac{\rho_{q,eff}(\lambda)}{1-\rho_{q,eff}(\lambda)\mathbf{r}^q(\lambda)}\mathbf{t}^{hem,q}_{bs}(\lambda)\le\delta(\lambda)\quad . \tag{F8}$$

This means that contribution of the ground (soil or/and understory) to the canopy leaving radiation is comparable to the uncertainty in the retrieved BHR and so there is not reliable information to estimate the Q_2 term. We neglect additional absorption within the canopy due to the interaction between the ground and canopy in this case and set $A^{hem}=\mathbf{r}^{hem}_{bs}$.

There is another problem encountering when one uses Eq. (F5) to evaluate the canopy absorptance. The term $1/\mathbf{t}^q$ in (F5) may become arbitrarily large as LAI is taken larger and larger. Although $(A^{hem}_{\mathrm{mod}el}-\mathbf{r}^{hem}_{bs})/\mathbf{t}^q$ tends to zero in this case, equation (F5) containing measured A^{hem} instead of modeled BHR tends to infinity as LAI value increases, namely,

$$\lim_{LAI\to\infty}\frac{A^{hem}(\lambda)-\mathbf{r}^{hem}_{bs}(\lambda)}{\mathbf{t}^q(\lambda)}=\lim_{LAI\to\infty}\frac{[A^{hem}_{\mathrm{mod}el}(\lambda)+\delta(\lambda)]-\mathbf{r}^{hem}_{bs}(\lambda)}{\mathbf{t}^q(\lambda)}=\lim_{LAI\to\infty}\frac{\delta(\lambda)}{\mathbf{t}^q(\lambda)}=\infty\quad . \tag{F9}$$

Thus, small variations in $A^{hem}_{\mathrm{mod}el}$ can cause numerical instabilities in the FPAR retrieval technique. Evaluation of FPAR for sufficiently dense canopies, therefore, requires special attention in order to avoid such instabilities.

It follows from Eqs. (101f), (101i) and (F5) that the canopy absorptance can be expressed as

$$\mathbf{a}^{hem}_{\mathrm{mod}el}(\lambda)=1-A^{hem}_{\mathrm{mod}el}(\lambda)-\left[\mathbf{t}^{hem,q\equiv1}_{bs}(\lambda)-\frac{\mathbf{t}^q(\lambda)+\mathbf{a}^q(\lambda)}{\mathbf{t}^q(\lambda)}(A^{hem}_{\mathrm{mod}el}(\lambda)-\mathbf{r}^{hem}_{bs}(\lambda))\right]\quad . \tag{F10}$$

The expression in the square brackets describes the fraction of radiation at the wavelength λ absorbed by the ground (soil and/or understory). It can take on non-negative values only, i.e., the following inequality holds true:

$$A_{\mathrm{mod\,el}}^{hem}(\lambda)-\mathbf{r}_{bs}^{hem}(\lambda)\le\frac{\mathbf{t}_{bs}^{hem,q\equiv1}(\lambda)\mathbf{t}^{q}(\lambda)}{\mathbf{t}^{q}(\lambda)+\mathbf{a}^{q}(\lambda)} \tag{F11}$$

Because

$$\lim_{LAI\to\infty}\left\{[A_{\mathrm{mod\,el}}^{hem}(\lambda)-\mathbf{r}_{bs}^{hem}(\lambda)]-\frac{\mathbf{t}_{bs}^{hem,q\equiv1}(\lambda)\mathbf{t}^{q}(\lambda)}{\mathbf{t}^{q}(\lambda)+\mathbf{a}^{q}(\lambda)}\right\}=0, \tag{F12}$$

inequality (F11) can be violated due to the retrieved uncertainty when we replace $A_{\mathrm{mod\,el}}^{hem}$ by A^{hem}. This takes place when LAI is sufficiently large. It follows from inequality (F11) and

$$\begin{aligned}\mathbf{a}_{\mathrm{mod\,el}}^{hem}(\lambda)&=\mathbf{a}_{bs}^{hem}(\lambda)+\frac{\mathbf{a}^{q}(\lambda)}{\mathbf{t}^{q}(\lambda)}\left[A_{\mathrm{mod\,el}}^{hem}(\lambda)-\mathbf{r}_{bs}^{hem}(\lambda)\right]\\&\le\mathbf{a}_{bs}^{hem}(\lambda)+\frac{\mathbf{a}^{q}(\lambda)}{\mathbf{t}^{q}(\lambda)}\cdot\frac{\mathbf{t}_{bs}^{hem,q\equiv1}(\lambda)\mathbf{t}^{q}(\lambda)}{\mathbf{t}^{q}(\lambda)+\mathbf{a}^{q}(\lambda)}\le\mathbf{a}_{bs}^{hem}(\lambda)+\mathbf{t}_{bs}^{hem,q\equiv1}(\lambda),\end{aligned} \tag{F13}$$

that the fraction of radiation absorbed by the ground becomes sufficiently small in this case. Thus, the violation of (F11) due to the retrieved uncertainty indicates that the contribution of the ground to the canopy absorptance does not exceed the retrieval uncertainty in A^{hem} and there is no reliable information to estimate the Q_2 term. We set $\mathbf{a}_{\mathrm{mod\,el}}^{hem}=\mathbf{a}_{bs}^{hem}$ in this case.

It follows from the above discussions that the following formula can approximates $\mathbf{a}^{hem}$ as accurate as the BHR is retrieved:

$$\mathbf{a}^{hem}(\lambda)=\begin{cases}\mathbf{a}_{bs}^{hem}(\lambda)+\dfrac{\mathbf{a}^{q}(\lambda)}{\mathbf{t}^{q}(\lambda)}\left[A^{hem}(\lambda)-\mathbf{r}_{bs}^{hem}(\lambda)\right] & \text{if}\quad 0<A^{hem}-\mathbf{r}_{bs}^{hem}<\dfrac{\mathbf{t}_{bs}^{hem,q\equiv1}\mathbf{t}^{q}}{\mathbf{t}^{q}+\mathbf{a}^{q}},\\ 1\text{-}A^{hem}(\lambda), \quad \text{otherwise.}\end{cases} \tag{F14}$$

Theorem. The inequality $\mathbf{a}^{hem}\le 1-A^{hem}$ is true.

This theorem shows that the proposed FPAR retrieval technique provides good agreement between two MISR products – the PAR-integrated BHR, A_{PAR}^{hem}, and FPAR.

Proof. Let $\varepsilon=A^{hem}-A_{\mathrm{mod\,el}}^{hem}$. Consider the situation when inequality (F11) takes place. We have

$$\mathbf{a}^{hem}(\lambda)=\mathbf{a}_{bs}^{hem}(\lambda)+\frac{\mathbf{a}^{q}(\lambda)}{\mathbf{t}^{q}(\lambda)}\left[A_{\mathrm{model}}^{hem}(\lambda)+\varepsilon-\mathbf{r}_{bs}^{hem}(\lambda)\right]=\mathbf{a}_{\mathrm{mod}\,el}^{hem}+\frac{\mathbf{a}^{q}(\lambda)}{\mathbf{t}^{q}(\lambda)}\varepsilon(\lambda)\quad. \tag{F15}$$

Substituting Eq. (F10) into Eq. (F15) and taking into account $A_{\mathrm{mod\,el}}^{hem}=A^{hem}-\varepsilon$ we get

$$\mathbf{a}^{hem}(\lambda) = 1 - A^{hem}(\lambda) + \varepsilon - \left[\mathbf{t}_{bs}^{hem,q\equiv 1}(\lambda) - \frac{\mathbf{t}^q(\lambda)+\mathbf{a}^q(\lambda)}{\mathbf{t}^q(\lambda)}(A^{hem}(\lambda) - \mathbf{r}_{bs}^{hem}(\lambda) - \varepsilon)\right] + \frac{\mathbf{a}^q(\lambda)}{\mathbf{t}^q(\lambda)}\varepsilon$$

$$= 1 - A^{hem}(\lambda) - \left[\mathbf{t}_{bs}^{hem,q\equiv 1}(\lambda) - \frac{\mathbf{t}^q(\lambda)+\mathbf{a}^q(\lambda)}{\mathbf{t}^q(\lambda)}(A^{hem}(\lambda) - \mathbf{r}_{bs}^{hem}(\lambda))\right] + \varepsilon - \frac{\mathbf{t}^q+\mathbf{a}^q}{\mathbf{t}^q}\varepsilon + \frac{\mathbf{a}^q}{\mathbf{t}^q}\varepsilon$$

$$= 1 - A^{hem}(\lambda) - \left[\mathbf{t}_{bs}^{hem,q\equiv 1}(\lambda) - \frac{\mathbf{t}^q(\lambda)+\mathbf{a}^q(\lambda)}{\mathbf{t}^q(\lambda)}(A^{hem}(\lambda) - \mathbf{r}_{bs}^{hem}(\lambda))\right].$$

It follows from inequality (F11) that the expression in the square brackets is positive. Therefore, $\mathbf{a}^{hem} \le 1 - A^{hem}$. **This completes the proof**.

Note if we set $\mathbf{a}^{hem} = \mathbf{a}_{bs}^{hem}$ when inequality (F11) was violated, we would get

$$\mathbf{a}^{hem}(\lambda) = \mathbf{a}_{bs}^{hem}(\lambda) \le \mathbf{a}_{bs}^{hem}(\lambda) + \frac{\mathbf{a}^q(\lambda)}{\mathbf{t}^q(\lambda)}\left[A_{\mathrm{mod\,el}}^{hem}(\lambda) - \mathbf{r}_{bs}^{hem}(\lambda)\right] = \mathbf{a}_{\mathrm{mod\,el}}^{hem}(\lambda) \quad .$$

It follows from Eq. (F10) that $\mathbf{a}_{\mathrm{mod\,el}}^{hem} \le 1 - A_{\mathrm{mod\,el}}^{hem}$ and, as a consequence, $\mathbf{a}^{hem} \le 1 - A_{\mathrm{mod\,el}}^{hem}$. It means that the uncertainty in $\mathbf{a}^{hem}$ is comparable to the uncertainty in BHR in the case of dense canopies.

3.3.7.2.2. Flow of the FPAR retrieval algorithm

For each candidate biome/canopy model passed the test, the FPAR retrieval algorithm first compute canopy absorptances $\mathbf{a}^{hem}$ at the MISR spectral bands as follows.

If a retrieved value of A^{hem} exists at wavelength λ_l then

$$\mathbf{a}^{hem}(\lambda_l, bio, lai, \mu_0) = \mathbf{a}_{bs}^{hem}(\lambda_l, bio, lai, \mu_0) + \frac{\mathbf{a}^q(\lambda_l, bio, lai)}{\mathbf{t}^q(\lambda_l, bio, lai)}\left[A^{hem}(\lambda, \mu_0) - \mathbf{r}_{bs}^{hem}(\lambda_l, bio, lai, \mu_0)\right],$$

if $0 < A^{hem}(\lambda_l, \mu_0) - \mathbf{r}_{bs}^{hem}(\lambda_l, bio, lai, \mu_0) < \dfrac{\mathbf{t}_{bs}^{hem,q\equiv 1}(\lambda_l, bio, lai, \mu_0)\mathbf{t}^q(\lambda_l, bio, lai)}{\mathbf{t}^q(\lambda_l, bio, lai) + \mathbf{a}^q(\lambda_l, bio, lai)}$, and

$\mathbf{a}^{hem}(\lambda_l, bio, lai, \mu_0) = 1 - A^{hem}(\lambda_l, \mu_0)$

otherwise. Here λ_1=446nm, λ_2=558nm and λ_3=672nm are the centers of the MISR spectral bands. Note that the variables $\mathbf{r}_{bs}^{hem}$, $\mathbf{a}_{bs}^{hem}$, $\mathbf{a}^q$ and $\mathbf{t}^q$ must be specified to evaluate the merit functions. Therefore, there is no need to prepare additional calculations in order to compute $\mathbf{a}^{hem}$.

If A^{hem} is unavailable, the following formula is used to evaluate the canopy absorptance at wavelength λ_l:

$$\mathbf{a}^{hem}(\lambda_l, bio, lai, \mu_0) = \mathbf{a}_{bs}^{hem}(\lambda_l, bio, lai, \mu_0) + \\ + \mathbf{a}^{q}(\lambda_l, bio, lai)\frac{\rho_{q,eff}(\lambda_l, bio, lai)}{1-\rho_{q,eff}(\lambda_l, bio, lai)\mathbf{r}^{q}(\lambda_l, bio, lai)}\mathbf{t}_{bs}^{hem,q}(\lambda_l, bio, lai, \mu_0)$$

Note that the ratio $f^{dir}(\lambda_l,\mu_0)$ is needed to estimate $\mathbf{t}_{bs}^{hem,q}$ $\mathbf{a}_{bs}^{hem}$ from Eqs. (101j) and (101k). Because this parameter is missing, we use a simulated value of f^{dir} in this case. The simulated ratio f^{dir} is stored in the CART file.

If the integrals in the Q_1 and Q_2 terms are treated in the same way as those for PAR-integrated quantities in Section 3.3.5, then

$$FPAR(bio, lai, \mu_0) = \frac{\sum_{l=1}^{3}\mathbf{a}^{hem}(\lambda_l, bio, lai, \mu_0)e_l^{hem}(\mu_0)\hat{w}_l}{\sum_{l=1}^{3}e_l^{hem}(\mu_0)\hat{w}_l} \quad ,$$

where $\hat{w}_l$ are given by Eq. (97). If e_λ^{hem} at wavelength λ_l is unavailable, a simulated value of the normalized incident irradiance is used. Simulated e_λ^{hem} are stored in the CART file.

It follows from the theorem that the PAR-integrated BHR does not exceed 1-*FPAR*, i.e., no any conflicts between two MISR products, the PAR-integrated BHR, A_{PAR}^{hem}, and FPAR, will occur. Now, if there is …. (as in Surface Retrieval ATB, p. 66).